

---

This is an electronic reprint of the original article.  
This reprint may differ from the original in pagination and typographic detail.

Vainio, Valtteri; Miettinen, Mikael; Majuri, Jaakko; Theska, René; Viitala, Raine  
**Manufacturing and static performance of porous aerostatic bearings**

*Published in:*  
Precision Engineering

*DOI:*  
[10.1016/j.precisioneng.2023.06.014](https://doi.org/10.1016/j.precisioneng.2023.06.014)

Published: 01/11/2023

*Document Version*  
Publisher's PDF, also known as Version of record

*Published under the following license:*  
CC BY-NC-ND

*Please cite the original version:*  
Vainio, V., Miettinen, M., Majuri, J., Theska, R., & Viitala, R. (2023). Manufacturing and static performance of porous aerostatic bearings. *Precision Engineering*, 84, 177-190.  
<https://doi.org/10.1016/j.precisioneng.2023.06.014>

---

This material is protected by copyright and other intellectual property rights, and duplication or sale of all or part of any of the repository collections is not permitted, except that material may be duplicated by you for your research use or educational purposes in electronic or print form. You must obtain permission for any other use. Electronic or print copies may not be offered, whether for sale or otherwise to anyone who is not an authorised user.



# Manufacturing and static performance of porous aerostatic bearings<sup>☆</sup>

Valtteri Vainio<sup>a,\*</sup>, Mikael Miettinen<sup>a</sup>, Jaakko Majuri<sup>a</sup>, René Theska<sup>b</sup>, Raine Viitala<sup>a</sup>

<sup>a</sup> Department of Mechanical Engineering, Aalto University, Espoo, Finland

<sup>b</sup> Precision Engineering Group, TU Ilmenau, Germany

## ARTICLE INFO

### Keywords:

Aerostatic bearing  
Air bearing  
Air bearing manufacturing

## ABSTRACT

According to the common body of knowledge, aerostatic bearings invariably need narrow manufacturing tolerances to ensure maximal load capacity and high stiffness. This study experimentally investigates the manufacturing of porous material aerostatic bearings and the effect of manufacturing parameters on the performance properties of the bearings. During the study, samples were manufactured using different methods, and the geometrical and performance properties of each sample were inspected. The bearing performance measurement device developed during the study is introduced. The results present the dependence between manufacturing parameters and bearing properties under varying load and operating pressure conditions. The results clearly suggest that effect of bearing surface roughness on load capacity is small; meanwhile, surface planarity has a major impact on load capacity.

## 1. Introduction

Aerostatic bearings are commonly applied to machinery where high-precision motion is necessary. Common examples include measuring devices such as coordinate measuring machines (CMM) and high speed spindles; however, aerostatic bearings are also applied to medical devices such as computer tomography scanners (CT scanners) and ultra-precision machine tools such as micro turning centers.

A major advantage with aerostatic bearings is the accurate and almost frictionless motion which produces minimal heat. Frictionless operation is beneficial for supporting emission reductions in order to meet the targets set for industrial machinery by the UN Sustainable Development Goals and The European Green Deal [1].

The development of advanced lubrication fluids and machinery motion systems, such as roller elements and journal bearings, has reduced energy consumption in rotational and translational machines [2]. Wider application of aerostatic bearings to machinery may reduce energy losses even more and decrease the maintenance needs of the associated machinery.

Aerostatic bearings have been studied widely and for a long time: the first aerostatic bearing was developed by Kingsbury in 1897 [3]. The utilization of aerostatic bearings in industrial solutions is low due to the relatively high price of aerostatic bearing systems and practical difficulties related to the technology. The origin of these disadvantages is mainly a lack of technological knowledge and missing research information.

Aerostatic bearings are commonly divided into categories according to the air feed, i.e., the restrictor structure. The two main categories are porous material restrictor and orifice restrictor bearings [4]. Porous materials are defined as materials which consist of a matrix of solid material that has internal voids, often referred to as pores. If these voids are interconnected, they allow flow, i.e., permeation of fluids through the material. This type of porosity is referred to as open porosity, and the measure classifying the amount of fluid flow is referred to as permeability. Porous material aerostatic bearings can be manufactured from any material that has suitable mechanical properties and suitable permeability for adequate air flow through the material. Graphite is the most common porous restrictor material used due to its beneficial properties in the case of unintentional contact between the porous restrictor and the opposing surface. The main advantage of porous aerostatic bearings is the even air feeding profile to the air gap through the restrictor material, as the graphite surface is practically full of microscopic holes; the air distribution to the air gap is homogeneous and thus the pressure distribution in the air gap is as uniform as possible [5]. Other materials, including ceramics or metal foams, such as sintered alumina have been proposed to be used as the base material in porous material aerostatic bearings. Sintered alumina is a synthetic material and its material matrix has a very regular structure, which is advantageous as it yields high similarity between manufacturing batches [6].

<sup>☆</sup> This paper was recommended by Associate editor Prof. R. Leach.

\* Corresponding author.

E-mail address: [valtteri.s.vainio@aalto.fi](mailto:valtteri.s.vainio@aalto.fi) (V. Vainio).

## Nomenclature

### Mathematical symbols

$\delta F$	Change of the force applied to the bearing
$\delta h$	Change of the air gap height
$\bar{x}$	Average of the measured samples
$h$	Air gap height
$h_{1-3}$	Length gauge reading from sensors 1–3
$h_{d1-d3}$	Deflection reading from sensors 1–3
$N$	Amount of the samples
$S$	Stiffness of the air film
$x_i$	Measured value
$(x_n, y_n, z_n)$	Gap measuring gauge coordinate

### Abbreviations

CT	Computer tomography
CMM	Coordinate measuring machine
DAQ	Data acquisition device
CNC	Computer numerical control
PCD	Polycrystalline diamond

Graphite has good friction properties against commonly used counter surface materials during undesired physical contact. In addition, during the contact of the bearing and the opposing surface, porous material bearing flow properties are not significantly changed. Meanwhile the nozzles of the orifice type bearing may be blocked.

Although the advantages of porous material aerostatic bearings are undisputed, orifice type aerostatic bearings are more widely adopted in commercial solutions, arguably because the orifice technology was developed earlier [7]. Orifice type bearings are highly sensitive to orifice size and geometry which makes them expensive to manufacture and highly sensible to scratches [8]. The orifice type, shape and location can be defined according to the application and favored properties. Several types of pockets and grooves can be used and they may also be combined into the feed system. These pocket and grooves, which increase air volume in the air gap reduce the damping properties of the bearing [9]. Porous type bearing allows higher bi-directional air flow compared to nozzle type bearings partially improving the performance properties of porous material bearings.

Aerostatic bearings utilize externally pressurized gas, commonly air, as a lubricant between the bearing element and the opposing surface. A high pressure air film separates the bearing element and the opposing surface, which makes the aerostatic bearing an almost ideal machine element when minimal friction and wear and high positioning accuracy are the main design objectives [10]. In addition, nitrogen and other gases can also be used as lubricants, although compressed air is often the most cost-effective solution. In some applications, various process gases can also be used in aerostatic bearings to avoid process contamination. Because aerostatic bearing systems have high accuracy and bearing elements can be damaged by impurities, the air fed into the system needs to be clean. The air source for aerostatic bearing systems is commonly an oil-free instrument air line, with higher air purity and more uniform pressure, separated from the common pressurized air network.

The thickness of the lubricating air film is commonly on the scale of  $2\ \mu\text{m}$  to  $10\ \mu\text{m}$ , which calls for high accuracy and extremely close tolerances for the aerostatic bearings themselves and for the systems utilizing the air bearings [9]. The requirements for the opposing surfaces are challenging: the surface needs to be stable and of high flatness. In addition, no corrosion is allowed and the opposing surface needs to be fail-safe for the bearing if contact occurs. Since the dimensions

of the opposing surface are larger than the dimensions of the bearing, the requirements are more difficult to fulfill. This sets demanding requirements for the manufacturing technology of the aerostatic bearing components. Machining graphite, the most common porous restrictor material, can be done with common machinery such as lathes, milling machines and grinders. However, graphite is a highly abrasive. Therefore, wear resistant tooling is required. Unsuitable tooling has high wear and, furthermore, the produced surface quality is coarser. Diamond tools are commonly used in graphite machining due to their high abrasive wear resistance [11].

Material removal in graphite cutting can be categorized into three main types, as presented in Fig. 1. The figure shows the microstructural deformation occurring in graphite during the machining process and thus explains the surface quality formed. In the case of manufacturing of aerostatic bearings, the desired mechanism is plastic deformation, depicted by type a, as it results in the smoothest surface. The properties of the graphite material are important when utilized for aerostatic bearing restrictor manufacturing because some graphite grades are more prone to type b and c mechanisms, and are thus unsuitable for smooth surface production [12].

Lapping is also a suitable surface finishing method for graphite based aerostatic bearings. Lapping can be executed against a separate lapping surface or against the bearing's own journal. Diamond or silicone based lapping compounds are commonly used to increase the material removal rate. In cases where the bearing profile is not a planar surface, the lapping is commonly executed against the bearing journal, e.g., in the case of cylindrical or spherical bearings [13,14]. In commercial production, the low time-efficiency of lapping has to be considered.

As stated earlier, aerostatic bearings are precision machine elements which have narrow manufacturing tolerances. Previous research considering porous material aerostatic bearings has mainly focused on the behavior of the most optimal designs. The published literature considering the manufacture of porous material aerostatic bearings is scarce and old [14]. Therefore, this study focuses on producing experimental data of porous material aerostatic bearing performance, with respect to the manufacturing method and final product tolerance.

In published literature, scientific experimental research results are often compared and analyzed with computational simulations. Publicly available simulation models are mainly applied for nozzle type bearings and hence cannot be utilized in this study [15,16].

The current body of knowledge lacks comparative research on different manufacturing methods, as well as analysis of the properties, such as planarity and performance, of the realized workpieces. Thus, the current study focuses only on flat circular aerostatic bearings and presents the following contributions beyond the state-of-the-art:

1. Measurement setup for aerostatic bearing performance characterization, including automated load and air gap measurement over a specified load range,
2. Nine sample set of aerostatic bearings manufactured using three different manufacturing methods utilizing three different graphite grades,
3. Experimental comparison and evaluation of the manufactured samples, in addition to one commercially available aerostatic bearing.

The present study unveils the connection between the different graphite grades, manufacturing methods and performance.

## 2. Methods

### 2.1. Performance test setup

A measurement device with a data acquisition system was designed and manufactured during this study to conduct the bearing performance measurements. Previous research has not presented a

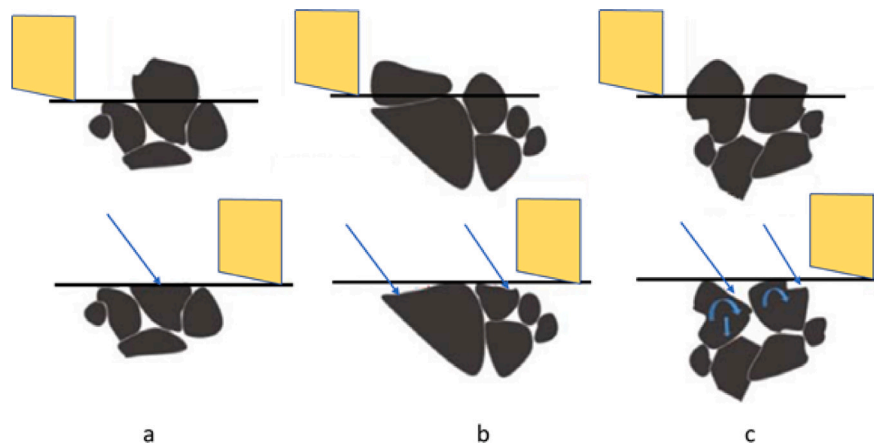


Fig. 1. During graphite cutting, three different microstructural deformation mechanisms occur. (a) plastic deformation, (b) brittle fracture and (c) grain rotation. The arrows indicate the effect of each mechanism on the graphite material. Source: Adapted from [12].

fully automated bearing performance measurement setup. The main goals of the design of the measurement setup were low measurement uncertainty and high automation level, to gain high quality results and eliminate human error. Furthermore, the fully automated measuring process enabled the possibility to produce a multi-point measurement data set effortlessly and in a repeatable manner.

The test setup developed during this study is presented in Fig. 2. Previously published studies utilized aerostatic bushings and ball joints to exert force on the sample bearing [17–19]. These structures can have backlash and have sliding friction in the contact zone of the machine elements. The developed test setup utilized flexural joints to reach an optimal structure with neither friction nor backlash. The bearing movement was arranged in its load-carrying direction with a four-bar-linkage compliant mechanism, the joints of which were flexural joints. The linkage mechanism restricted all other degrees of freedom except the vertical direction. There is obviously a slight parasitic motion due to the 4-bar-linkage. However, the parasitic motion is negligible due to the short movement in the primary motion direction, and the optimal angle of the linkages in the measurement position. The flexure unit was manufactured by milling and electrical discharge machining from a 316l Duplex stainless-steel billet. The flexure unit has an integrated movement limiting feature which prevents over travel that could damage the mechanism by plastic deformation. The alignment of the bearing against the natural stone surface was ensured using a second flexure unit, presented in Fig. 3, which has two circular flexure features with a 90 degree phase difference to enable the bearing to have rotational degrees of freedom.

A natural stone cube was used as the bearing opposing surface in the measurement setup. The cube surfaces were lapped and its manufacturer gives  $0.5 \mu\text{m}$  as a maximum Ra value for the surface roughness, while the average surface roughness depth Rz is specified to be no more than  $3 \mu\text{m}$ . The flatness of the surfaces was specified to be less than  $1 \mu\text{m}$ .

The bearing load was applied with a precision pneumatic cylinder that had a very low internal friction due to its metallic seals. The diameter of the piston was 40 mm. The seals between the piston and the cylinder are metal rings producing an intentional small leakage, which, according to the manufacturer, results in minimal friction. Due to this special structure, the force control accuracy of the cylinder is 0,05 N and no stick-slip phenomena occurs. Pressure regulation for the load cylinder was conducted using a Festo pressure regulator which had 0–10 bar range and  $\pm 1\%$  FS accuracy. The whole pneumatic system is described in Fig. 4.

The bearing load produced with the pneumatic cylinder was also measured with a force sensor placed between the bearing and the pneumatic actuator. The force sensor was an HBM U2B with a 10 kN

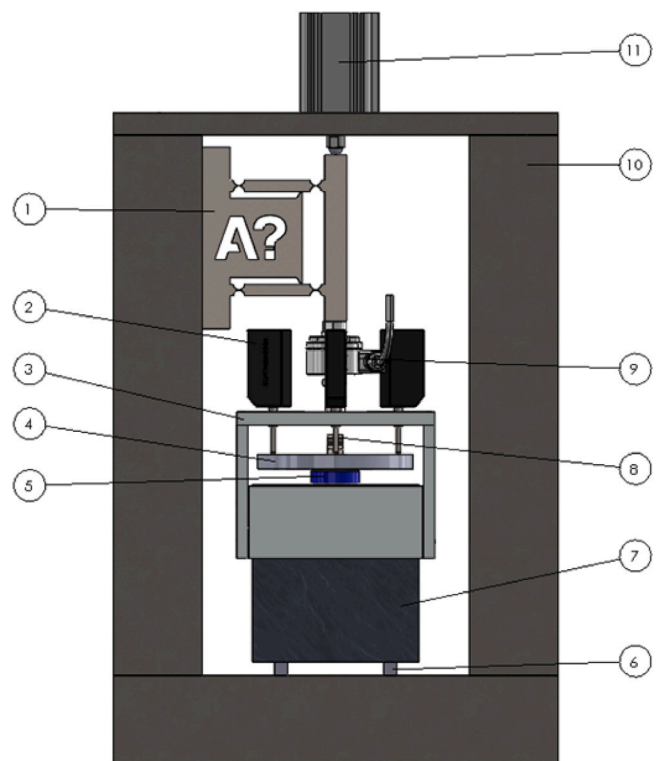


Fig. 2. Drawing of the test setup. (1) Four bar linkage with flexures, (2) Heidenhain MT-12 length gauge, (3) Measurement frame, (4) Measuring area extension plate, (5) Aerostatic bearing, (6) Stone block spacers, (7) Stone block, (8) Flexure to align bearing with stone block, (9) Force sensor, (10) Load frame, (11) Low friction pneumatic cylinder.

measuring range and accuracy of  $\pm 1\%$  FS and it was calibrated up to 1 kN using a series of known weights. The load sensor was aligned with the centerline of the bearing. The force measuring systems does not take into account the measuring force of linear length gauges, and weights of sample, measuring area extension plate and the sample aligning flexure. the measuring force of Heidenhain MT-12 sensor is 0,5 – 0,75 N depending on the displacement of the measuring head. Thereby the force can be considered negligible. Moreover, as the work is considered as comparison between the samples rather than measuring absolute values, the setup remains valid. Fig. 5 presents the assembly of the force



Fig. 3. Flexure unit with two circular shaped flexures that is used to enable rotational degrees of freedom for the bearing. This unit was used to ensure parallelism between the top surface of the stone cube and the surface of the aerostatic bearing.

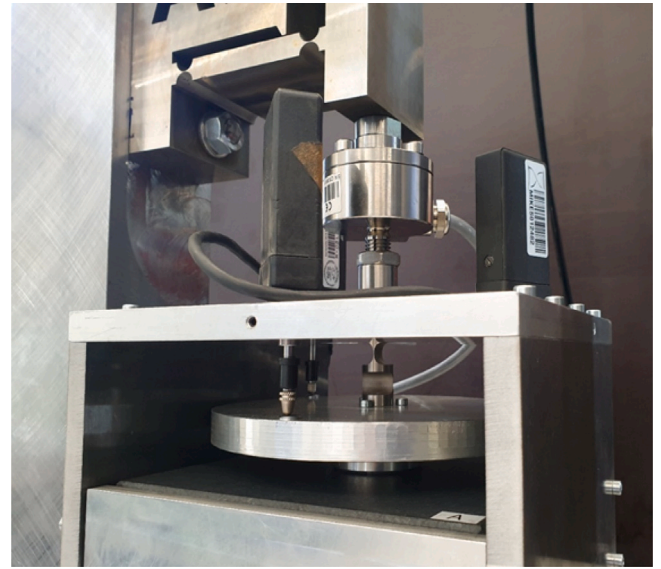


Fig. 5. Force sensor is mounted on the bottom of the four-bar linkage unit, and a loading rod transfers the load through the second flexure into the bearing.

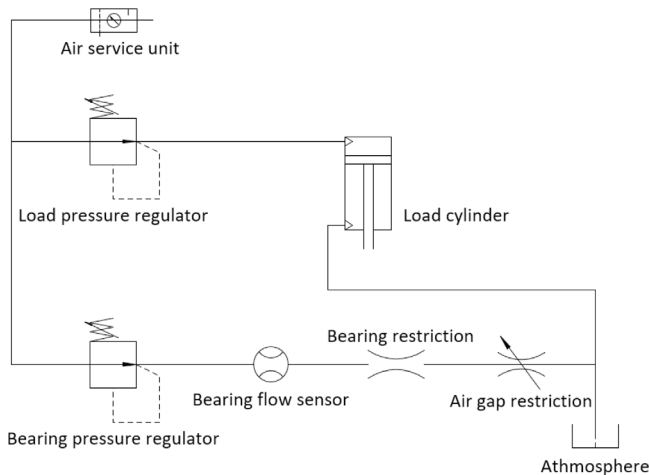


Fig. 4. Pneumatic system of the measurement device includes two pressure regulators; one for the load cylinder and one for the bearing supply. The flow to the bearing is measured with a separate sensor.

sensor and Table 1 presents the types of control and measuring signals on the measuring setup.

The air gap height between the bearing and the bearing surface was measured using three Heidenhain MT-12 displacement sensors. MT-12 sensors have 12 mm measuring range and an accuracy of  $\pm 0,2 \mu\text{m}$ . The sensors were mounted on a separate measurement frame independent from the loading frame. Physical separation of the measurement frame and the loading frame increases the accuracy of the system by blocking the effect of frame flexing on the measuring results. The measuring frame was supported with three spheres on the opposing sides of the stone cube.

A circular aluminum disk was placed between the loading rod and the aerostatic bearing, which allowed the displacement sensors to be

located further away from the center of the bearing in order to have a clearance for the force sensor. To avoid the effect of material surface roughness, displacement sensors are in contact with ground steel inserts embedded into the aluminum disk.

The pressure regulator for the bearing supply pressure was similar to the regulator used with the load cylinder despite the pressure range being 0–6 bar. The flow to the bearing was measured using a SMC PFM7-50-C6-E flow sensor which has a 1–50 l/min range and  $\pm 5\%$  FS accuracy.

### 2.2. Air film stiffness

Deflection of the system, which includes the aerostatic bearing, is highly dependent on the stiffness of the air film between the aerostatic bearing and its opposing surface. The static stiffness of the aerostatic bearing can be calculated according to the next equation, similarly to the stiffness of conventional bearing systems [20]:

$$S = \frac{\delta F}{\delta h} \quad (1)$$

where  $S$  is the stiffness of the air film,  $\delta F$  is the change of the force applied to the bearing and  $\delta h$  is the change of the air gap height.

### 2.3. Data acquisition and processing

The data acquisition and control system was based on a National Instruments USB-DAQ 6215 and Matlab code which controlled the measurement process. The device was used to log the air flow, force and pressure sensor readings and control the pressure regulators. The measurement program collected and logged the data into measurement files. Further, Matlab was used to process the measuring data and plot the result graphs.

Heidenhain MT-12 linear length gauges were interfaced to an EIB 742 module and read using the C packages provided by Heidenhain. The sensors were mounted with a 120-degree angular difference around the test sample, which enabled an arithmetic average of the readings to be taken to enhance the air gap height measurement accuracy.

**Table 1**

Bearing flow sensor reading was collected directly using a DAQ device. The signal from the force transducer signal amplifier was analog and was received with the DAQ device. The signal from the length gauges was analog and was received with an evaluation electronics unit which was connected to a computer with an Ethernet cable.

Device	Model	Range	Sensitivity	Accuracy	Signal type	Receiver
Bearing flow sensor	SMC PFM7-50-C6-E	1–50 l/min	–	±5%FS	Analog	–
Force transducer	HBM U2B	10 kN	2 mv/V	±1% FS	Wheatstone bridge	HBM AE-101
Length gauge	Heidenhain MT-12	12 mm	–	±0,2 μm	Digital	Heidenhain EIB 742
Loading cylinder pressure regulator	Festo VPPM-6L-L-1-G18-0L10H-V1P-S1C1	0–10 bar	–	±1% FS	Analog	–
Bearing supplypressure regulator	Festo VPPM-6L-L-1-G18-0L6H-V1P-S1C1	0–6 bar	–	±1% FS	Analog	–

#### 2.4. Planarity measurements

The surface planarity of all samples was measured using a Zeiss C700 CMM. Measuring points were located on circles around the center point of the sample; the diameter of the first measuring circle was 1.5 mm and the other circles were located 3 mm apart until the edge of the sample. The measuring points located on these circles 3 mm apart resulted in 237 measuring points per bearing sample.

#### 2.5. Roughness measurements

Surface roughness measurements were carried out with Bruker ContourGT-K optical profiler. Three measuring points were located in the center of the sample bearing, in the middle point of the radius of the sample and at the edge of the sample bearing. From these points, a square area with size of 1 mm by 1 mm was sampled. From these sampled areas, arithmetic average was calculated and used as a surface roughness of the sample bearing.

#### 2.6. Manufacturing methods

The aerostatic bearings examined in the present study were constructed from two components: an aluminum frame and a porous graphite restrictor. All of the used samples were similar, with 37 mm graphite restrictor diameter and a 4.5 mm thickness. The aluminum frames were machined and the graphite inserts were coarsely pre-machined before the assembly of the bearing. Fig. 7 presents the internal features of the bearing frame, before the graphite restrictor was glued in place. The graphite inserts were glued to the bearing frames with a two-component epoxy glue and after curing, the bearing surface of the graphite was machined so that the samples were similar in dimensions and the bearing surface was planar and parallel to the back of the aluminum frame. The bearing frames were manufactured with narrow tolerances which ensured the similarity of the samples after finishing operations. The finish machining was conducted using a CNC lathe equipped with soft jaws (Fig. 6), which were specially manufactured to mount the samples. The soft jaws were machined to the same diameter as the external diameter of the bearing frame to avoid deformation of the bearing frame during machining; furthermore, a more secure grip could be achieved with a lower gripping force compared to hard jaws. Machining was executed using a polycrystalline diamond (PCD) tool without coolant.

Lapping was conducted with a CNC milling machine by rubbing the sample against a stone surface. Surface planarity, measured by the cube manufacturer, is stated as 0.75 μm on the stone surface used for lapping. The lapping procedure consisted of two combined maneuvers: the sample was in circular plane motion with a 90 mm diameter and at the same time the sample was rotated around its center point. The speed for the circular plane motion was approximately 1000 mm/min and the rotating speed of the sample was 60 rpm. Fig. 8 presents the lapping setup. The tool holder used in the milling machine was a tap holder which applied a constant spring load to the bearing through a ball-nose pin mounted on the holder. An air-blast was aimed at the stone surface to remove most of the debris from the process.



Fig. 6. Bearing faces were machined using a CNC lathe equipped with soft jaws, the gripping diameter of which corresponded to the external diameter of the bearing.



Fig. 7. The bearing frames had internal channels to distribute the air flow evenly to the graphite insert.

#### 2.7. Test samples

The test samples inspected in this study were manufactured in-house, excluding one commercially available unit which was used as

**Table 2**

Material data for graphites used in sample manufacturing. The supplier of material Q did not provide pore size and open porosity data.

Grade	Particle size	Pore size	Open porosity	Density
A	5 μm	0,8 μm	85 %	1.73 g/cm <sup>3</sup>
T	10 μm	1,5 μm	85%	1.82 g/cm <sup>3</sup>
Q	7 μm	N/A	N/A	1.83 g/cm <sup>3</sup>

**Table 3**

Sample bearing configurations. Feed 1: 0.16 mm/rev feed 230 m/min cutting speed. Feed 2: 0.08 mm/rev feed 300 m/min cutting speed. The lapped samples were first machined with the parameters of Feed 2.

Graphite grade	A			T			Q		
	A lapped	A fine	A rough	T lapped	T fine	T rough	Q lapped	Q fine	Q rough
Feed 1			x			x			x
Feed 2	x	x		x	x		x	x	
Lapped	x			x			x		



**Fig. 8.** The lapping process was performed using a CNC milling machine. The bearing sample was rubbed against the stone surface and an air-blast aimed at the process to remove debris. The tool used to hold the sample, was a ball-nose shaft which allowed the surfaces to align.

a reference. Three graphite grades with varying porosity and particle sizes were used. All the test samples were machined using a CNC lathe by using two cutting speed and feed combinations and furthermore half of the samples with a smoother surface were also lapped. **Table 3** presents the in-house manufactured samples and **Table 2** provides the configurations for the materials used in the test samples.

**2.8. Procedure of the experiment**

The measurement of each sample consisted of three main phases:

1. Short circuit flow measurement
2. System deflection measurement
3. Air gap height and air flow measurement with varying bearing supply pressure and varying load

The short circuit flow was measured by connecting the bearing to the pressure supply and hoisting it 1.5 mm above its opposing surface. The air gap was large enough to have negligible restriction in this configuration, thus all the restriction was from the graphite. Furthermore, as there is a possibility of applied bearing load to deflect the measuring device itself, system deflection measurement was carried out. Aim of this phase was to exclude the possible system deflection from the actual characterization measurement data of the test samples. Deflection of the system was measured by setting the bearing supply

pressure to zero and measuring the artificial negative air gap with all of the used bearing loads. The used bearing supply pressures were 3, 4, 5 and a 6 bar and the load applied to the bearing varied between 0 N and 775 N with an increment of 25 N between the measuring points. The air gap height and flow were measured at each measuring point. **Fig. 9** presents the structure of the test process including an explanation of all sub-phases.

The following equation explains how the air gap heights were derived from the length gauge readings and the system deflection values:

$$h = \frac{(h_1 - h_{d1}) + (h_2 - h_{d2}) + (h_3 - h_{d3})}{3} \tag{2}$$

where  $h$  is the air gap height,  $h_{1-3}$  are the length gauge readings from sensors 1–3 and  $h_{d1-d3}$  are the length gauge readings during system deflection measurement with same bearing load.

Bearing slant plane was determined with the method of least squares. Least square regression plane is given as:

$$z = ax + by + c \tag{3}$$

where constants  $a$ ,  $b$  and  $c$  can be determined by minimizing equation:

$$G(a, b, c) = \sum (z_n - ax_n - by_n - c)^2 \tag{4}$$

where in turn  $(x_n, y_n, z_n)$  are coordinates of gap measurement length gauges. The gauges are distributed on a 65 mm diameter circle with 120 degrees between them. This gives us know  $x$  and  $y$  coordinates, whereas  $z$  coordinate is the gauge reading. Angle of the bearing can then be calculated as an angle between the opposing surface normal and slant plane normal with equation:

$$\cos(a, b) = \frac{\vec{a} \cdot \vec{b}}{|\vec{a}| |\vec{b}|} \tag{5}$$

where  $\vec{a} \cdot \vec{b}$  is the dot product between opposing surface normal vector and slant plane normal vector,  $|\vec{a}|$  and  $|\vec{b}|$  are the length of the vectors.

**3. Results**

The results of the present study are presented in five sections. The first section consists of the deflection measuring results which are utilized to generate the bearing performance results in the following sections. The second section presents the results of all the test samples measured with a 6 bar bearing supply pressure. Other bearing supply pressures are not presented because of the high similarity of the results. In Section 3.3 the measuring results from the second section are arranged and evaluated against each other, which forms the performance index for each sample. The last section presents the results of the surface planarity and roughness measurements conducted for the samples and furthermore explains the performance of each sample.

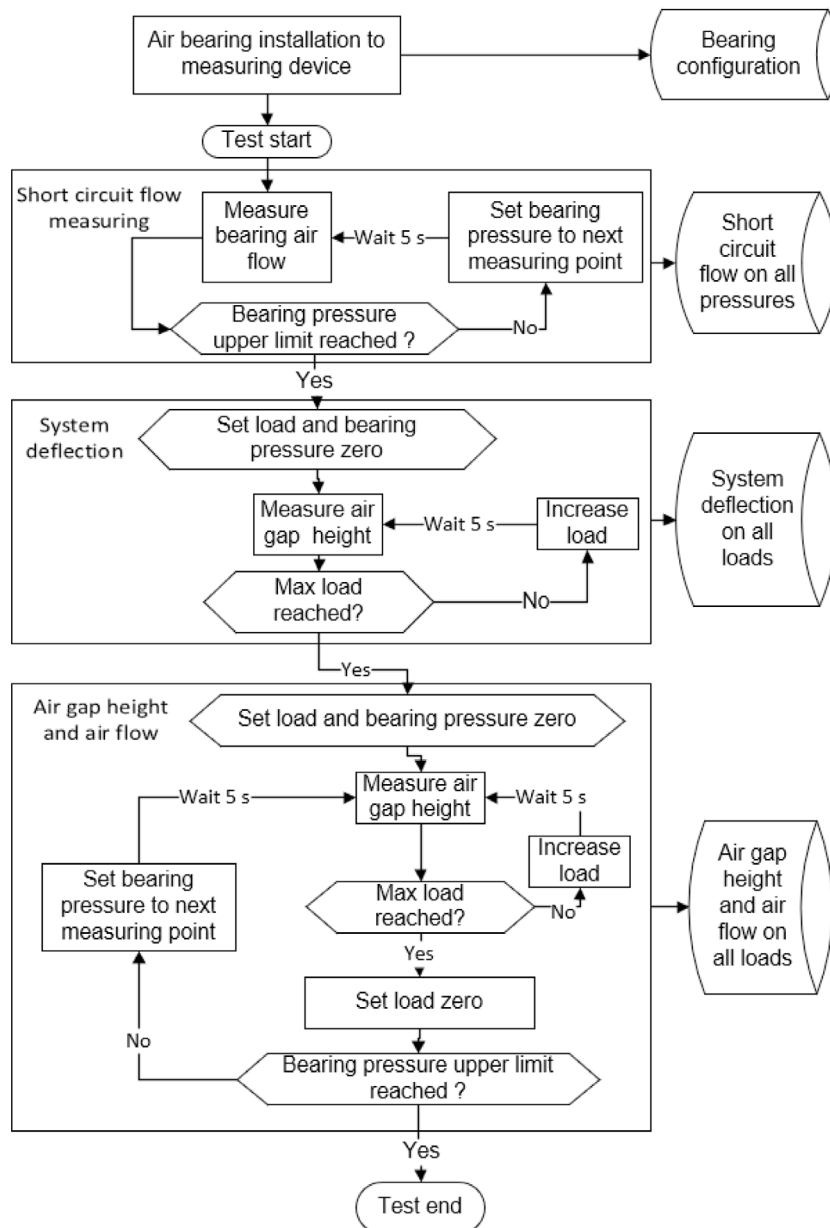


Fig. 9. Procedure of the measuring experiment including three main phases: 1. Short circuit flow measurement, 2. System deflection measurement, 3. Air gap height and air flow measurement with varying load and supply pressure.

### 3.1. Deflection

System deflection was measured after each sample was installed in the measuring setup. Deflection between samples may vary because of errors or impurities in the installation or imperfections and variation in the bearing samples. For example, variations in the process of gluing the graphite insert to the bearing frame may cause variation in the sample stiffness. Moreover sample-specific deflection measuring results correspond to the system calibration after each sample change. The system deflection was measured by setting the bearing supply pressure to zero and increasing the bearing load from 0 N to 750 N in 30 N increments. After each increment, the system was allowed to stabilize for thirty seconds before the measurement. The linear gauge readings were acquired at each load increment, and the overall system deflection was calculated by taking the arithmetic average of the gauge readings. Fig. 10 presents the deflection of the measurement system for all samples.

### 3.2. Load, flow and air gap measurements

The highest allowed pressure for commercially available aerostatic bearings is commonly 6 bar, which was also used as the highest pressure in this study. Fig. 11 presents the relationship between the load applied to the bearing and the air gap height at a 6 bar bearing supply pressure.

Fig. 12 presents the air flow through the bearing samples at different air gap heights at a 6 bar bearing supply pressure.

Fig. 13 presents short circuit flow of the samples. Short circuit flow measurements were carried out in the absence of opposing surface, therefore allowing free air flow through the bearing.

Fig. 15 presents the tilting angles of the bearings at given gap height.

The stiffness for all the samples was calculated according to Eq. (1) and the results are presented in Fig. 14. The x-axis is limited on the figure to present only air gaps of 1 μm and higher, because with smaller

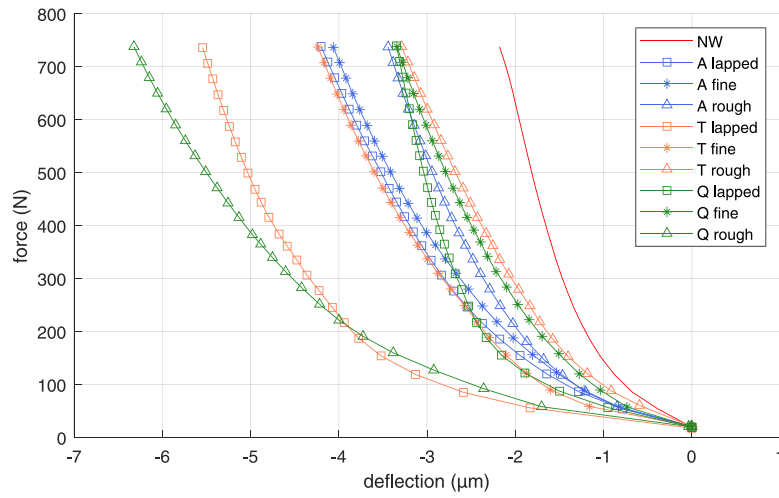


Fig. 10. Deflection of the measurement system with a 0 bar bearing supply pressure. Sample NW is commercially available reference sample and the rest of the samples are in house made.

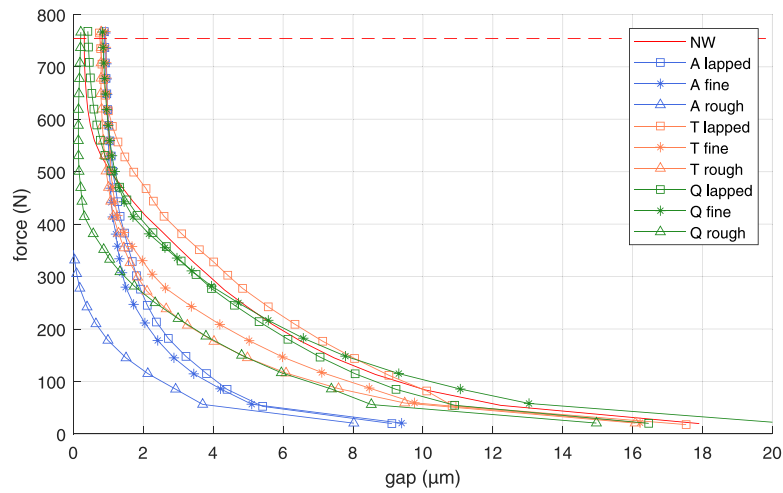


Fig. 11. Air gap height and bearing load with a 6 bar bearing pressure. The red horizontal dashed line presents the theoretical maximal load and is calculated using the bearing supply pressure and surface area.

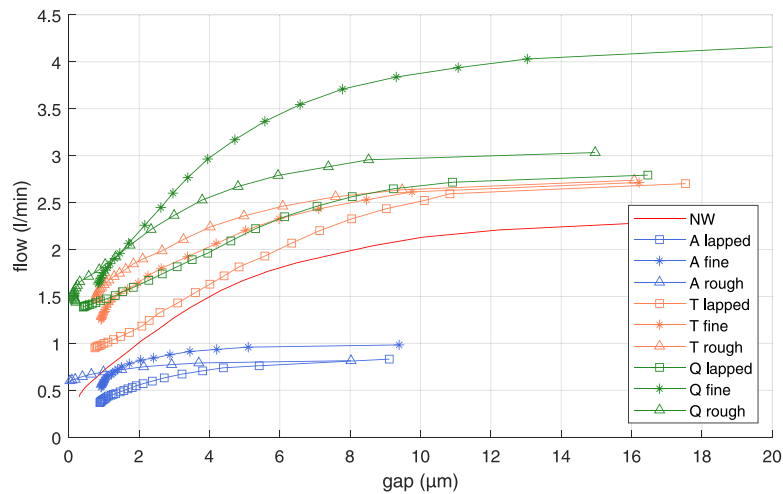


Fig. 12. Height of the air gap and air flow through the bearing at a 6 bar bearing supply pressure.

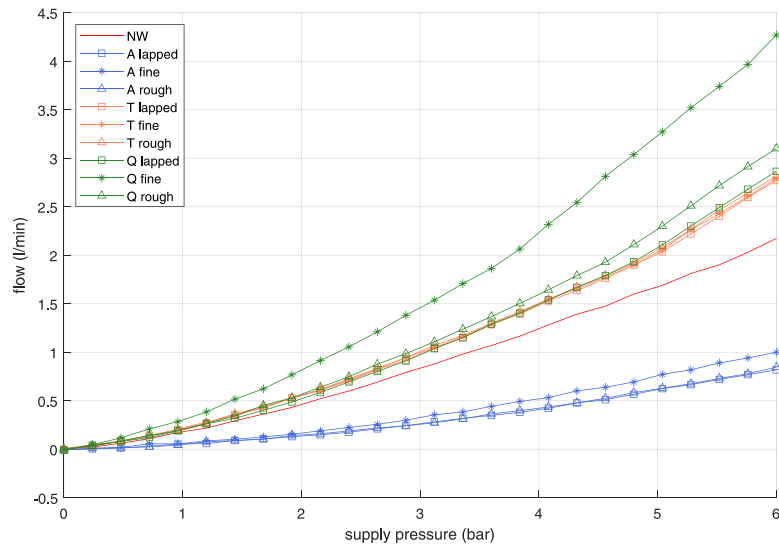


Fig. 13. Short circuit flow of the samples.

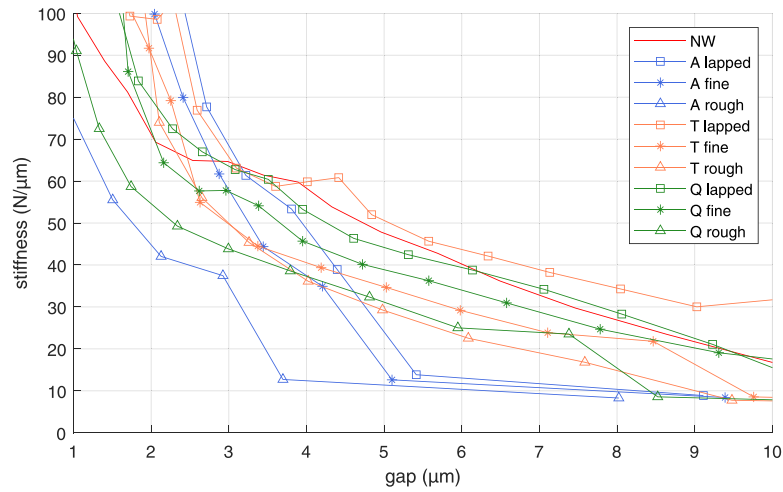


Fig. 14. Stiffness of the aerostatic bearing system at a 6 bar bearing supply pressure.

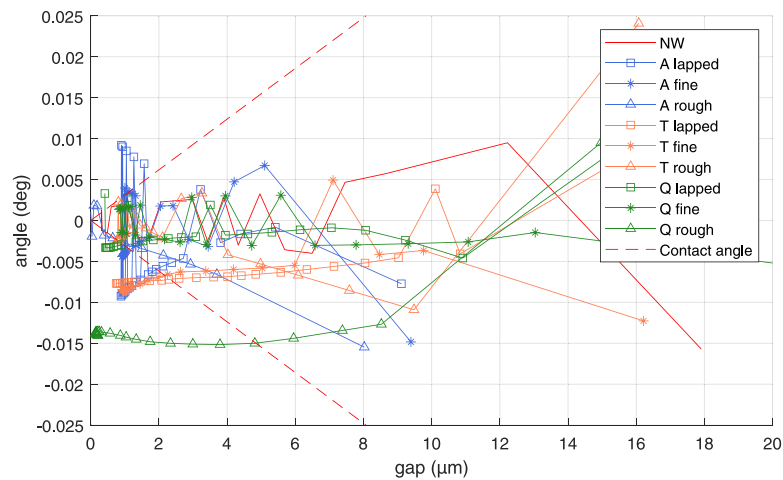


Fig. 15. Bearing slant angles in relation to the normal of opposing surface at 6 bar bearing supply pressure. Dashed red line indicates contact angle, a calculated value at which bearing edge will start to contact the opposing surface.



Fig. 16. Test samples. (1) T lapped, (2) T fine (3) Q lapped (4) Q fine (5) NW.

Table 4

Surface roughness  $R_a$  at each measuring point. An average surface roughness is measured over the diameter of the sample and averaging is conducted by the measuring device.

Sample name	Center	8 mm from center	15 mm from center	Average
A lapped	0,226	0,129	0,370	3,724
A fine	1,440	1,532	1,497	3,483
A rough	2,236	1,989	2,179	2,276
T lapped	0,450	0,633	0,518	1,419
T fine	1,703	1,656	1,704	1,790
T rough	2,140	1,982	2,454	2,478
Q lapped	0,460	0,426	0,409	0,758
Q fine	1,660	1,781	1,709	2,200
Q rough	2,953	2,636	2,664	2,704
NW	0,404	0,400	0,406	0,525

air gaps the calculated stiffness rather presents the stiffness of the whole measurement system.

### 3.3. Surface planarity and roughness

The surface planarity of the samples is presented in Fig. 17 where the samples are evaluated according to the highest peak-to-peak result. The surface roughness measuring results are presented in Table 4. As explained in earlier section, surface roughness measuring results presents measured  $R_a$  values of the samples at the center of the sample, 8 and 15 mm of from the center and also an average value.

Despite the lapping time being extended according to properties of the material, materials with lower machinability did not reach similar surface properties to those of samples manufactured from material with better machinability. Some of the test samples are presented in Fig. 16 to present this phenomenon.

Material Q with good machinability reached highly similar surface properties compared to the commercially available sample. Furthermore, the lapped sample manufactured from Material T did not reach a smooth surface roughness nor shine despite having the longest lapping time.

The surface planarity and roughness of each sample was measured as described in the Methods section. Fig. 17 presents the surface planarity and Table 4 presents the surface roughness measuring results of the samples.

## 4. Discussion

### 4.1. Analysis of the measuring device

As explained earlier, the whole measurement system was developed and built during this study. The aims for the system developed were high automation level and low uncertainties. These targets were mainly reached: the device and the measurement system operated as designed and the uncertainties, analyzed later, were small.

To reach even higher accuracy, some mechanical interfaces on the device should be improved to even more optimal type. The support of

the stone cube was arranged with two steel spacers between the cube and the frame which moreover was not as stiff and stable an arrangement as it could have been. The optimal solution from the perspective of system stiffness would be one sphere the middle under the cube. The sphere should take contact to the cube through a plate which includes cone-shaped counterbore for the sphere. This arrangement furthermore disables the effect of surface imperfections on the system stability and shear forces do not occur to the stone cube. The difficulty with one sphere support is its mechanical instability in a case where the sphere contact point does not align with the direction and reduced center line of the bearing force applied to the cube. A compromise could be a three-sphere system between the cube and the measuring frame. The spheres should be located as close to each other as possible to avoid shear forces occurring on the stone cube.

### 4.2. Analysis of the results

The highest load-carrying capacity was observed on the samples with the most planar surfaces, which is relatively obvious according to previously published literature. The difference in static load-carrying capacity between the best lapped samples and the best machined samples is surprisingly small. Knowledge based on the state-of-the-art review would suggest a remarkably higher difference between samples; lapping should yield much better load-carrying capacity. However, only the static performance of the bearings was analyzed; the situation might be different under dynamic conditions. These results contribute to the question of tolerance requirements in porous material aerostatic bearing manufacturing. Furthermore, when comparing the load capacities of the samples to the surface planarity, there seems to be clear correlation. Even when the surface planarity is only estimated as one remainder value between the top and bottom measuring values, the most planar surface seems to have the highest load capacity. Load capacity seems to decrease simultaneously with decreasing surface planarity.

According to the results, surface roughness seems to have a significant effect on the bearing air flow. Fig. 12 presents the flow rate for the samples, and samples manufactured from the same material

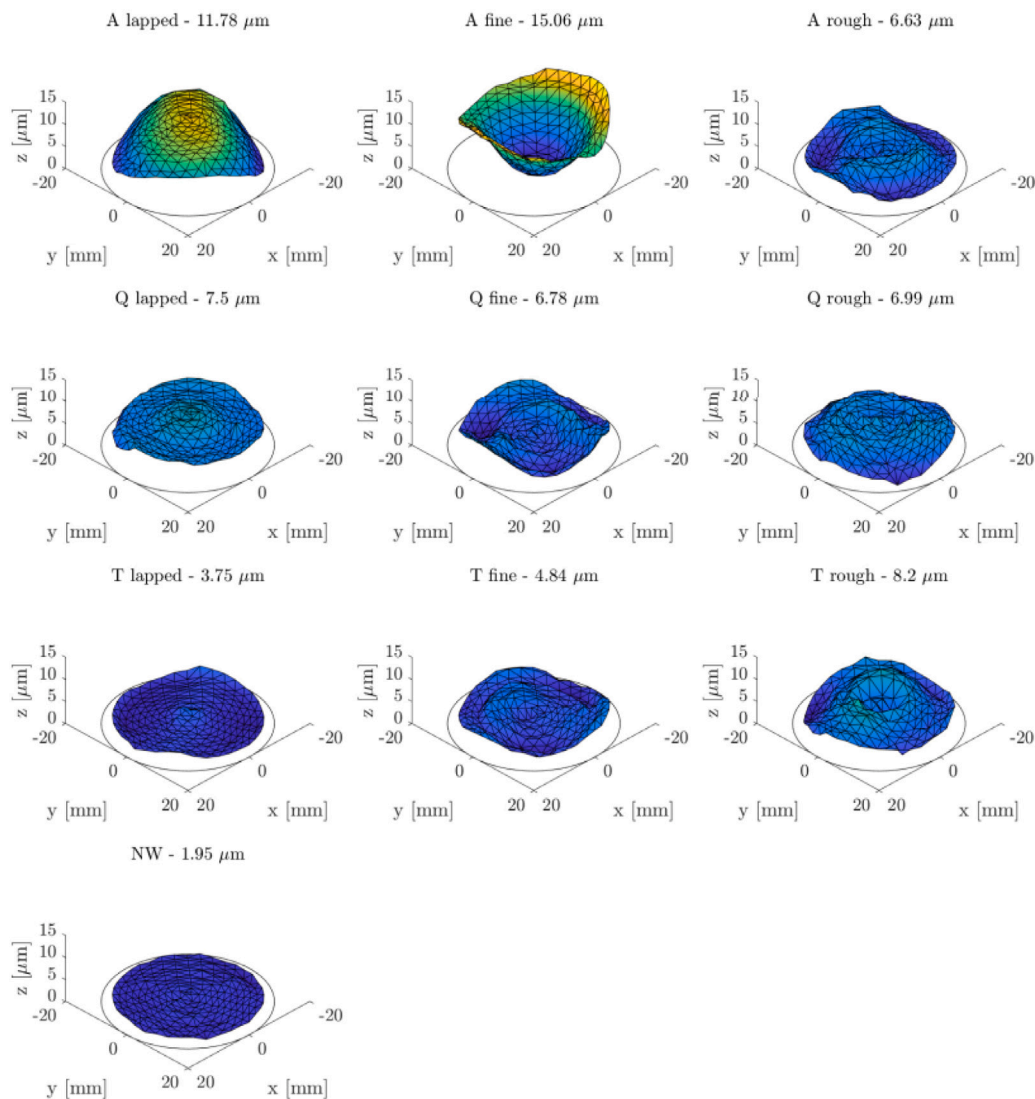


Fig. 17. The surface planarity of each sample was measured using a CMM and no supply air was fed to the samples.

with different methods seem to have highly dissimilar flow rate values. Lapped samples have the smoothest surface and thus the smallest open volume between the sample and the opposing surface due to the minimal amount of surface irregularities. Open volume means the free volume remaining between the sample and the opposing surface. This causes the air gap to have higher stiffness, since the open volume is smaller and therefore compresses less than with samples having rougher surface. With an air gap height below  $1.5\ \mu\text{m}$ , the samples manufactured from each material seem to have a similar order in the flow rates: the sample with the coarsest surface has the highest flow rate. Furthermore, with larger air gap height, the “fine” samples seem to have the highest or at least as high flow rate as the “rough” samples. As different sample materials expressed similar behavior between “fine” and “rough” samples, meanwhile having distinct planarity, surface geometry does not, at least solely, explain higher flow rate growth of the “fine” sample in proportion to gap height. No simple explanation for this phenomenon may exist, but the microscale deformations in the graphite surface during the machining process may be one possible reason.

With lower air gap heights, many samples may have a physical contact between it and the opposing surface, as seen from Fig. 15. The slant angle varies significantly between different samples and air gap heights. The most probable reason for the variation is different surface planarities of the samples. For example, “A lapped” sample

has a convex surface according to Fig. 17. The surface shape makes the sample labile, which explains the large angle oscillation and even physical contact on the opposing surface. On the other hand, samples “Q lapped” and “Q fine” have relative planar surfaces and behave similarly to the commercially available sample with low variation and contact only at very low gap heights. Furthermore, sample “T lapped” has the most planar surface apart from the commercial sample. The sample did, however, contact the opposing surface more than “Q lapped”, even though it otherwise had very small angle variation. Why the most planar sample did not perform the best is probably due to the different graphite grade. As seen from Fig. 12, Q material allows more air to seep through the graphite than T material. Therefore, it seems that the air flow through the “T lapped” is not sufficient to keep the sample off the surface at lower gap heights. In Fig. 11 it is clearly seen that zero air gap is not reached with all samples. This is intuitive as the surface planarities of some samples are higher than the remaining air gap. Consequently the absolute zero air gap height is complex to determine.

Methods and devices presented in this study are only capable of indirect estimation of contact occurring between the sample and opposing surface. Therefore air gap height measurements performed with interferometer is considered in Section 4.5.

Short circuit flow rates present clear difference between samples made of same material. Manufacturing of the samples named with

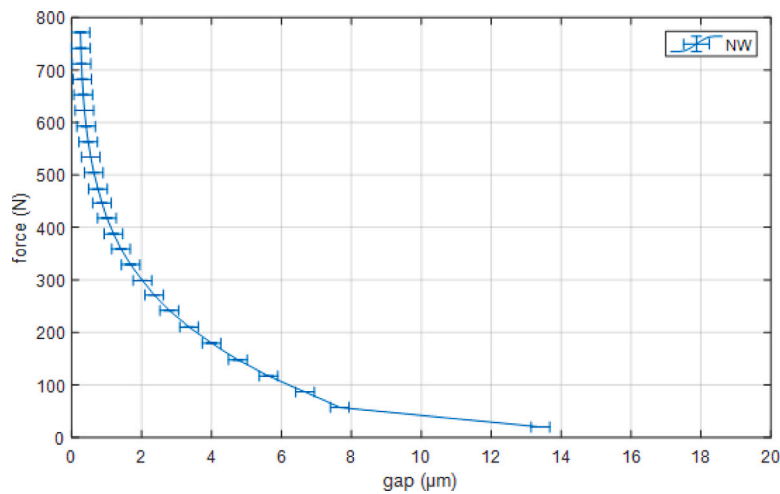


Fig. 18. Standard uncertainty of the force and air gap height measuring results. The uncertainty is calculated from 10 repeated measurements with the sample “NW”.

“rough” included only one turning round with higher cutting feed and speed meanwhile “fine” and “lapped” samples were first turned with smaller cutting feed and speed. Afterwards “lapped” samples were also lapped. Samples “lapped” and “fine” are therefore similar in the view of manufacturing until the lapping is conducted. From the results, it can be seen, that the lapping decreases the airflow at any given pressure. For material grades A and Q the effect is stronger, and for T also measurable. As can be seen from the results, fine machined samples had higher flow compared to rough machined and lapped samples. As described in 1, machining of the graphite may deform the microstructure in several ways. Deformation may occur in several layers, starting from the surface and reaching deep inside of the graphite. This deformation explains the difference of short circuit flow between samples manufactured from the same material. Main issue whilst analyzing short circuit flows is the lack of information related to short circuit flow through unmachined or unprocessed graphite. Because lapped samples are similar compared to fine machined samples before lapping, it is clear that lapping as a process decreases the flow through graphite. The reason for the decreased flow rate can be that either lapping closes the pores of the graphite or lapping reveals new surface which is not affected by fine machining. Although the material removal during lapping is minimal, the theory of pore closing is more probable. Second possible explanation is that with parameters used on fine machining, graphite pores are significantly more open after machining compared to lapping and rough machining. This may mean that lapping and rough machining results the graphite surface to be close to its nominal flow properties.

The properties of the porous material used to manufacture the sample had the highest impact on the bearing properties. The graphite grades were chosen to have different properties in the samples and similarly to have wide measuring data. The results clearly show that Material A had too low permeability, while the samples manufactured from Materials T and Q had highly similar permeability properties to the commercially available bearing sample.

The machinability of the graphite grades differed significantly; moreover, the samples manufactured from grades A and T did not reach a smooth surface even after long lapping periods. As seen from the results, the surface planarity had a major effect and the surface roughness a minor effect on the bearing properties. Material T is the most suitable graphite grade, considering the bearing performance, for aerostatic bearings out of the three tested materials.

The results show, that in the deflection measurement, there is no clear consistency between the surface finish method and the amount of resulted deflection. This may derive from the inconsistency of the gluing of the graphite to the bearing, planarity of the bearing frame or realized bearing surface planarity.

#### 4.3. Measurement uncertainties

The mechanical structure of the measuring device was designed to minimize uncertainty in the measurement process by selecting the optimal mechanical contacts between the elements of the device. The contact between the stone cube and the measuring frame was arranged with three spheres against a planar surface, which decreased the errors caused by geometrical imperfections. Error bars are not included in the result figures because the uncertainties of the results are separately presented and the core of the research is not in the measuring technology.

Errors caused by the sensors are categorized as a standard uncertainty and occur as a systematic error in the measuring results. The force transducer amplifier was calibrated during the measurements, while the rest of the sensors used the factory calibration. The force transducer amplifier was calibrated by the author, using accurately known masses to load the force transducer. The maximum error on the measuring range during calibration was 2.5 N. The standard uncertainty determination was executed by repeating the measuring process presented in Fig. 9 ten times with the sample “NW”. The standard uncertainty type in the system was determined by utilizing Type A evaluations [21]. First the standard deviation  $S(y)$  was calculated using the equation:

$$S(y) = \sqrt{\frac{1}{N-1} \sum_{i=1}^N (x_i - \bar{x})^2} \quad (6)$$

where  $N$  is the amount of measured samples,  $x_i$  is the measured value of the sample and  $\bar{x}$  is the average of the measured values at the measuring point.

The standard uncertainty can be calculated using the equation:

$$u(y) = \frac{S(y)}{\sqrt{N}} \quad (7)$$

Fig. 18 presents the standard uncertainty of the measurements. The maximum value for standard uncertainty in the air gap height measurement was  $0.5306 \mu\text{m}$  and in the force measuring  $0.5687 \text{ N}$ . The uncertainties for the air gap height and for the force measurements are negligible and the results of the study hold.

#### 4.4. Scientific impact

Graphite is a widely applied material especially in electroerosive machining electrodes. Also nuclear technology widely utilizes graphite and high-quality research on graphite machining is easily available. Porous material aerostatic bearings have been in industrial use since

the 1970s and the first manufacturing processes that are presented in publications are from that time period [13]. However, the state-of-art review indicates that no later publications on graphite based aerostatic bearing manufacturing processes are available. Despite the same manufacturing processes applied to common graphite components being able to be used in aerostatic bearing manufacturing, the current study demonstrates the effect of the manufacturing process on the properties of the bearing which is a totally novel research perspective. Graphite based aerostatic bearings are offered to the free market by a highly limited number of manufacturers, which limits the amount of available research information.

#### 4.5. Further research

The current study has produced a wide understanding of the basic principles of porous material aerostatic bearing manufacturing. Samples manufactured with different surface properties indicated the effect of the manufacturing method on the bearing properties. Because the lapped samples seem to have the best properties as bearings, further research should focus on improving the manufacturing process. Manufacturing of the samples investigated during the present study was relatively slow, which furthermore guides research to produce similar or better surface properties faster. No abrasive was used; instead, the surface porosity of the natural stone was used as the cutting media. Therefore, the material removal rate was low as the surface of the stone is very planar and smooth. Use of lapping compounds which include abrasive particles would improve the efficiency of the process. However, porous graphite absorbs fluids and embeds particles easily. Abrasive particles embedded in the graphite may ruin the opposing surface during the manufacturing process.

The measurements of the present study were conducted under static loading conditions. Further research will also include measurements that could prove the operational properties of the bearing under dynamic load conditions. Investigating the dynamic stiffness of the bearings is important for many practical applications of the bearings. Thus, the produced results show that the used samples have high load-carrying capacity and stiffness, but the situation may differ in dynamic conditions.

Published scientific literature presents several simulation models for aerostatic bearing system simulations [15]. These simulation models are mainly focused on nozzle type aerostatic bearings, which has ignited the development of a Computational Fluid Dynamics model suitable for porous material aerostatic bearings [22].

As said earlier, estimating the contact between the sample and opposing surface with devices and methods used in this study, results in an indirect process, in which the deflection of the device, and sample surface planarity and roughness serve as a major uncertainty source. Future research will include air gap height measurements performed with an interferometer, revealing the full air gap height distribution of the samples.

## 5. Conclusion

In the current study, the effect of the manufacturing properties of porous material aerostatic bearings on the performance of the bearings was investigated. The measurement setup and data acquisition system were designed and built. The main goals with the measurement system were to reach high accuracy and automation level to reliably produce a large dataset of the performance of the bearing samples. The results seem to have feasible uncertainties according to the uncertainty scrutinization, which confirms that the targets set regarding the measurement system were reached.

The bearing samples were manufactured and all bearing surfaces finished in-house. Turning with a diamond tool and lapping were used as the finishing methods for the samples. Furthermore, the manufactured samples had consistent properties: the properties, such as the

dimensions, which should be similar between samples were highly similar and properties, such as the surface roughness, which should differ between samples were dissimilar. The chosen sample properties and the sample quality supported the study and high-quality results were produced.

The target was to produce numerical data on the effect of bearing manufacturing parameters, including bearing material, for bearing load capacity and other operational properties. The current body of knowledge seemed to lack experimental research on the effect of material and manufacturing parameters on porous aerostatic bearing performance. This study established a novel dataset and analysis to bridge that gap. In addition an automated and low uncertainty measurement setup was developed and built. The automation level of the measurement setup removes human errors and ensures equal treatment of all samples. The measurement setup can be considered unprecedented in the literature. The current study reached this target extremely well and even proved that the surface quality has a relatively low effect on the bearing properties.

## Declaration of competing interest

The authors declare that they have no known competing financial interests or personal relationships that could have appeared to influence the work reported in this paper.

## Acknowledgments

This research was funded by the Academy of Finland, Finland as a part of the AI-ROT project (grant number 335717). The research was funded also by the 19ENG07 Met4Wind project, which has received funding from the EMPIR programme co-financed by the Participating States and from the European Union's Horizon 2020 research and innovation programme. Additionally, the research was also funded by Yrjö ja Senja Koivusen säätiö.

## References

- [1] European Commission. The European green deal. 2020, URL: [https://ec.europa.eu/info/sites/info/files/european-green-deal-communication\\_en.pdf](https://ec.europa.eu/info/sites/info/files/european-green-deal-communication_en.pdf).
- [2] Holmberg K, Andersson P, Nylund NO, Mäkelä K, Erdemir A. Global energy consumption due to friction in trucks and buses. *Tribol Int* 2014;78:94–114. <http://dx.doi.org/10.1016/j.triboint.2014.05.004>.
- [3] Kingsbury A. Experiments with an air-lubricated journal. *Am Soc Mech Eng* 1897;9(2):267–92.
- [4] Gao Q, Chen W, Lu L, Huo D, Cheng K. Aerostatic bearings design and analysis with the application to precision engineering: State-of-the-art and future perspectives. *Tribol Int* 2019;135:1–17. <http://dx.doi.org/10.1016/j.triboint.2019.02.020>.
- [5] Nield DA, Bejan A. Convection in porous media. fifth ed.. New York: Springer International Publishing; 2017, <http://dx.doi.org/10.1007/978-3-319-49562-0>.
- [6] Kwan YBP. Processing and fluid flow characteristics of hot isostatically pressed porous alumina for aerostatic bearing applications (Ph.D. thesis), Cranfield university; 1996.
- [7] Stout KJ, Rowe WB. Externally pressurized bearings - design for manufacture Part 1 - journal bearing selection. *Tribology* 1974;7(3):98–106. [http://dx.doi.org/10.1016/0041-2678\(74\)90009-8](http://dx.doi.org/10.1016/0041-2678(74)90009-8).
- [8] Belforte G, Colombo F, Raparelli T, Trivella A, Viktorov V. Comparison between grooved and plane aerostatic thrust bearings: static performance The nu-merical model considers a general formulation of the. *Meccanica* 2011;46:547–55. <http://dx.doi.org/10.1007/s11012-010-9307-y>.
- [9] Wardle F. Ultra precision bearings. Elsevier; 2015, p. 442. <http://dx.doi.org/10.1016/C2013-0-16179-X>.
- [10] Muzakkir SM, Hirani H. Maintenance free bearings. In: Proc. efficiency from bearings, lubrication and seals conference. Vol. 2. No. March 2015. 2015, p. 1–5. <http://dx.doi.org/10.17950/ijer/v4s3/311>, (Leeds, U.K.: Jun.8-10, 1976).
- [11] Tankus K, Tascioglu E, Atay G, Brunken H, Kaynak Y. The effect of cutting parameters and cutting tools on machining performance of carbon graphite material. *Mach Sci Technol* 2020;24(1):96–111. <http://dx.doi.org/10.1080/10910344.2019.1701020>.

- [12] Yan J, Heidari M. Fundamental characteristics of material removal and surface formation in diamond turning of porous carbon. *Int J Addit Subtract Mater Manuf* 2017;1(1):23. <http://dx.doi.org/10.1504/ijasm.2017.10003952>.
- [13] Rasnick WH. Air-bearing slides for precision X-Y turning machines. Technical Report, United States Atomic Energy Commission; 1971.
- [14] Rasnick WH. Air-bearing rework and impregnation. Technical Report, United States Atomic Energy Commission; 1972.
- [15] Colombo F, Lentini L, Raparelli T, Viktorov V, Trivella A. On the static performance of concave aerostatic pads. In: *Advances in mechanism and machine science*. 2019, p. 3919–28.
- [16] Gao S, Cheng K, Chen S, Ding H, Fu H. CFD based investigation on influence of orifice chamber shapes for the design of aerostatic thrust bearings at ultra-high speed spindles. *Tribol Int* 2015;92:211–21. <http://dx.doi.org/10.1016/j.triboint.2015.06.020>.
- [17] Connor BO. Performance characterization of porous graphite air bearings. Technical Report, Pennsylvania state university; 2002.
- [18] Khatait JP, Lin W, Lin WJ. Design and development of orifice-type aerostatic thrust bearing. Vol. 6. No. 1. Technical Report, SIMTech technical reports; 2005, p. 7–12.
- [19] Colombo F, Lentini L, Raparelli T, Trivella A, Viktorov V. Dynamic characterization of rectangular aerostatic pads with multiple inherent orifices. *Tribol Lett* 2018;66(4):133. <http://dx.doi.org/10.1007/s11249-018-1087-x>.
- [20] Slocum AH. *Precision machine design*. Prentice hall; 1992, p. 750.
- [21] Joint Committee For Guides In Metrology. JCGM 100:2008. GUM 1995 with minor corrections. *Evaluation of measurement data — Guide to the expression of uncertainty in measurement*. 2008, p. 134.
- [22] Plante JS, Vogan J, El-Aguizy T, Slocum AH. A design model for circular porous air bearings using the 1D generalized flow method. *Precis Eng* 2005;29(3):336–46. <http://dx.doi.org/10.1016/j.precisioneng.2004.11.011>.



**Valteri Vainio** was born in 1995. He received his M.Sc. degree in mechanical engineering from Aalto University in 2021. Currently, he is pursuing a D.Sc. degree in mechanical engineering at Aalto University. In his Master's thesis, he investigated the manufacturing and performance measurement of porous material aerostatic bearings. Current research topics include porous aerostatic bearings with a focus on manufacturing methods.



**Mikael Miettinen** was born in 1995. He received his M.Sc. degree in mechanical engineering from Aalto University in 2020, where he is currently pursuing a D.Sc. degree in mechanical engineering. In his Master's thesis, he developed an aerostatically sealed pressure chamber. His current research topics include porous aerostatic bearings and seals with a focus on applications with large rotors.



**Jaakko Majuri** was born in 1997. He received his B.Sc. degree in mechanical engineering from Aalto University in 2021, where he is currently pursuing a M.Sc. degree in mechanical engineering. In his Master's thesis, currently under progress, he is developing aerostatic bearing solutions to be used in heavy machinery.



**René Theska** was born in 1957. He received his degrees Dipl.-Ing. (1983) and Dr.-Ing. (1989) in Precision Engineering from TH Ilmenau/ TU Ilmenau, Germany. He worked in the industry from 1990 until 2001. Most of this time he worked on tactile and optical CMM technology as the head of R&D at Hexagon Metrology in Wetzlar, Germany. In 2001, he was appointed as Professor for Precision Engineering at TU Ilmenau. His research focus is on ultra-precision devices for the measurement of length, force and torque.



**Raine Viitala** was born in 1992. He received his M.Sc. and D.Sc. degrees in mechanical engineering from Aalto University in 2017 and 2018, and was appointed Assistant Professor in 2020. His doctoral dissertation was acknowledged with the Aalto University School of Engineering dissertation award. In 2018, Viitala visited Technische Universität Darmstadt researching rotating kinetic energy storages, i.e., flywheels. Viitala has a solid background in experimental large rotor research, including vibration analysis, bearing excitations, roundness measurements and manufacturing for operating conditions. His work is widely applied in several industrial applications, such as electric motors and generators, turbines, and paper machines. He instructs students at all academic levels, and is the responsible teacher of the Mechatronics minor at Aalto University.